Applied Physics Letters

Nonreciprocal thermal radiation of nanoparticles via spin-directional coupling with reciprocal surface modes

Cite as: Appl. Phys. Lett. **119**, 021104 (2021); https://doi.org/10.1063/5.0057446
Submitted: 20 May 2021 • Accepted: 01 July 2021 • Published Online: 13 July 2021

Jian Dong, Wenjie Zhang and Linhua Liu

Applied Physics Letters ARTICLE scitation.org/journal/apl

Nonreciprocal thermal radiation of nanoparticles via spin-directional coupling with reciprocal surface modes

Cite as: Appl. Phys. Lett. **119**, 021104 (2021); doi: 10.1063/5.0057446
Submitted: 20 May 2021 · Accepted: 1 July 2021 ·
Published Online: 13 July 2021

Jian Dong,[1,2,a)] Wenjie Zhang,[1,2] and Linhua Liu[1,2,a)]

AFFILIATIONS

[1]School of Energy and Power Engineering, Shandong University, Jinan, Shandong 250061, China
[2]Optics and Thermal Radiation Research Center, Shandong University, Qingdao, Shandong 266237, China

[a)]**Authors to whom correspondence should be addressed:** dongjian@sdu.edu.cn and liulinhua@sdu.edu.cn

ABSTRACT

We demonstrate nonreciprocal far-field thermal emission and nonreciprocal near-field radiative heat transfer of Weyl semimetal nanoparticles when the circular thermal emission of the particles directionally couples with the spin of the surface modes supported by a reciprocal substrate. Our work can be applied to the development of nonreciprocal and directional thermal emitters and to the nanoscale routing of a radiative heat flux.

Thermal radiation is a ubiquitous phenomenon that is important in numerous scientific and engineering disciplines. However, thermal radiation occurring in most situations, including the thermal emission of objects and the radiative heat transfer (RHT) between objects, is constrained by the Lorentz reciprocity. By reciprocity, the thermal emission of an object will be balanced by its absorption, which is specified by Kirchhoff's law[1] that the directional spectral emissivity equals to the directional spectral absorptivity, i.e.,

$$\varepsilon(\omega, \hat{\mathbf{r}}) = \alpha(\omega, \hat{\mathbf{r}}). \tag{1}$$

Here, ω is the angular frequency and $\hat{\mathbf{r}}$ denotes a specific direction. In the RHT between two objects, which is generally expressed as[2]

$$P_{ij} = 3\int_0^\infty \frac{d\omega}{2\pi}\left[\Theta(\omega, T_j)\mathcal{T}_{ij}(\omega) - \Theta(\omega, T_i)\mathcal{T}_{ji}(\omega)\right], \tag{2}$$

reciprocity imposes that the transmission coefficients are equal, i.e., $\mathcal{T}_{ij}(\omega) = \mathcal{T}_{ji}(\omega)$. Here, $\Theta(\omega, T)$ is the temperature-dependent Planck oscillator and P_{ij} is the net radiative heat flux from object j to i. Exploring ways to break the constraint of reciprocity in thermal radiation is of fundamental importance and may provide novel applications and management of thermal photons.[3]

Recently, nonreciprocal thermal radiation is attracting growing interest. The most investigated method to break the Lorentz reciprocity is to use nonreciprocal materials. Nonreciprocal far-field thermal emission and absorption, i.e., the violation of Kirchhoff's law, have been predicted in surface nanostructures containing magneto-optical (MO) materials that support nonreciprocal surface modes or guided modes under an external static magnetic field.[4–6] Very recently, violation of Kirchhoff's law is also predicted in surface structures made of topological Weyl semimetals (WSMs), which has the advantage of not requiring an external magnetic field.[7–9] The WSM exhibits anomalous Hall effect and takes asymmetric dielectric tensor like that of MO materials under an external magnetic field.[10,11] In parallel, nonreciprocal near-field RHT has been predicted in many-particle systems[12–16] due to the near-field many-body interaction and the nonreciprocal responses of MO or WSM materials. Moreover, nonreciprocal RHT between two nanoparticles, or equivalently a radiative thermal diode, can be realized via the near-field coupling between the particle and nonreciprocal surface modes.[17–19]

In this Letter, we predict the nonreciprocal thermal emission and RHT of nanoparticles when the particle emits circularly polarized waves (or thermal spin photons) and couples with propagating surface modes that are generally reciprocal. It has been investigated both theoretically and experimentally[20] that evanescent surface waves have intrinsic transverse spin, and surface waves traveling along opposite directions will have opposite spin-direction. Thus, unidirectional surface modes can be excited if circularly polarized incident light matches the spin of the surface modes in one direction, as illustrated in Fig. 1. Within this physical context, we will demonstrate that a nanoparticle

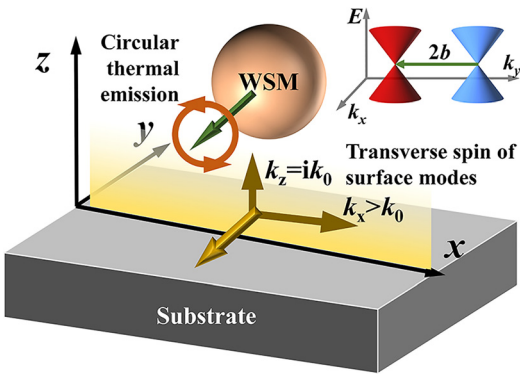

FIG. 1. Schematic of the spin-directional coupling between circular thermal emission and reciprocal surface modes; a Weyl semimetal (WSM) spherical nanoparticle is used as the circular thermal emission source.

thermally radiating circularly polarized light can directionally couple with the surface modes of a substrate, which is responsible for the nonreciprocal thermal radiation of the nanoparticle.

We choose a spherical WSM nanoparticle as the circular thermal emission source. Like MO nanoparticles,[21,22] the spherical WSM nanoparticle will exhibit circular dipole momentum and emit circularly polarized light without an external magnetic field. The dielectric tensor of WSMs with the momentum-separation 2**b** along the negative y direction adopts the form[10,11]

$$\hat{\varepsilon} = \begin{bmatrix} \varepsilon_d & 0 & i\varepsilon_a \\ 0 & \varepsilon_d & 0 \\ -i\varepsilon_a & 0 & \varepsilon_d \end{bmatrix}. \tag{3}$$

Here, $\varepsilon_a = be^2/2\pi^2\hbar\omega$ and $\varepsilon_d = \varepsilon_b + i\sigma/\omega$, where σ is the bulk conductivity given by[10,11]

$$\sigma = \frac{r_s g}{6}\Omega G\left(\frac{\Omega}{2}\right) + i\frac{r_s g}{6\pi}\left\{\frac{4}{\Omega}\left[1+\frac{\pi^2}{3}\left(\frac{k_B T}{E_F(T)}\right)^2\right] + 8\Omega\int_0^{\xi_c}\frac{G(\xi)-G\left(\frac{\Omega}{2}\right)}{\Omega^2-4\xi^2}\xi d\xi\right\}, \tag{4}$$

where ε_b is the background permittivity, $\Omega = \hbar(\omega + i\tau^{-1})/E_F$ is the complex frequency normalized by the chemical potential, τ^{-1} is the scattering rate corresponding to Drude damping, $G(E) = n(-E) - n(E)$ with $n(E)$, the Fermi distribution function, E_F is the chemical potential, $r_s = e^2/4\pi\varepsilon_0\hbar\nu_F$ is the effective fine structure constant, ν_F is the Fermi velocity, g is the number of Weyl points, and $\xi_c = E_c/E_F$ with E_c, the cutoff energy. We choose the parameters $b = 1\times10^9\ \mathrm{nm}^{-1}$, $g = 2$, $\tau = 1000$ fs, $\varepsilon_b = 6.2$, $\nu_F = 2\times10^5$ m/s, $\xi_c = 3$, and $E_F = 150$ meV, which are all in the range of theoretically or experimentally determined values.[10,11]

The radius R of the spherical WSM nanoparticle is assumed to be much smaller than the characteristic thermal wavelength so that the nanoparticle can be modeled as an electric dipole. The electric dipole polarizability tensor $\hat{\alpha}$, neglecting the radiative correction, is given by the Clausius–Mossotti formula $\hat{\alpha} = 4\pi R^3(\hat{\varepsilon}-\hat{1})(\hat{\varepsilon}+\hat{2})^{-1}$. For $\hat{\varepsilon}$ given in Eq. (3), $\hat{\alpha}$ adopts the form

$$\hat{\alpha} = \begin{bmatrix} \alpha_{xx} & 0 & \alpha_{xz} \\ 0 & \alpha_{yy} & 0 \\ -\alpha_{xz} & 0 & \alpha_{xx} \end{bmatrix}. \tag{5}$$

The nondiagonal element α_{xz} is responsible for the circular momentum, and the particle will emit circularly polarized light along the y direction in this case.[21,22] Figure 2(a) shows the real and imaginary parts of α_{xz} normalized by $4\pi R^3$. The peak and valley of the Re(α_{xz}) correspond to two localized circular modes of the WSM nanoparticle with opposite spin-directions, respectively.[21,22] We choose cubic boron nitride (c-BN) as the substrate, and its dielectric function is described by the Drude–Lorentz model[23] $\varepsilon(\omega) = \varepsilon_\infty(\omega_L^2 - \omega^2 - i\Gamma\omega)/(\omega_T^2 - \omega^2 - i\Gamma\omega)$, with $\omega_L = 2.45\times10^{14}$ rad·s, $\omega_T = 1.96\times10^{14}$ rad·s, $\Gamma = 9.93\times10^{11}$ rad·s, and $\varepsilon_\infty = 4.46$. c-BN is a reciprocal material, whose Reststrahlen band overlaps with the circular mode of the WSM nanoparticle at higher frequencies, as shown by the gray region in Fig. 2(a).

We first consider the spatial distribution of the thermally emitted electric field by a WSM nanoparticle above a c-BN substrate. The

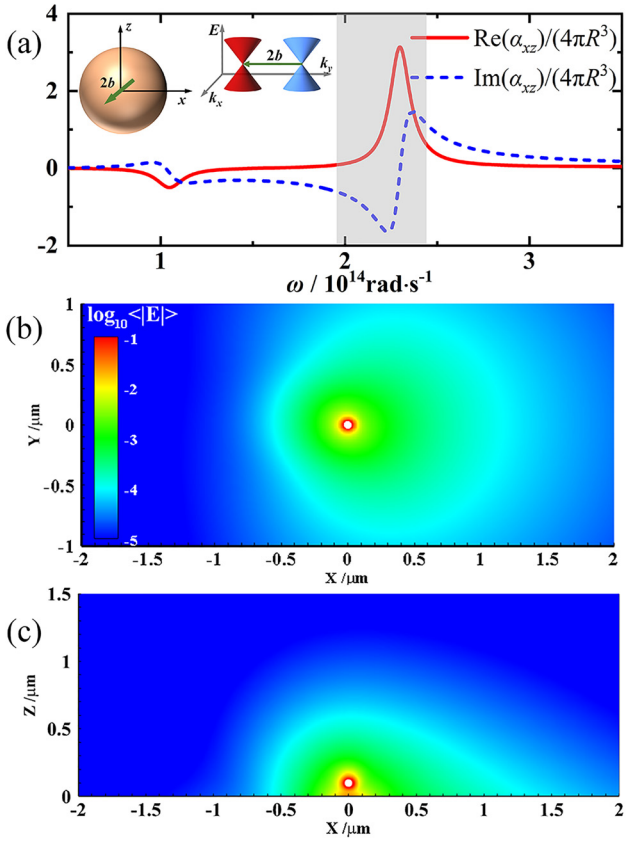

FIG. 2. (a) The α_{xz} component of the electric polarizability tensor of the WSM nanoparticle in vacuum (2b along the -y direction), the gray region shows the Reststrahlen band of c-BN; (b) xy-plane distribution of the averaged electric field $\langle|\mathbf{E}(\mathbf{r})|\rangle$ thermally emitted by a WSM nanoparticle ($R = 25$ nm) that locates above a c-BN substrate by a distance $h = 100$ nm, the frequency is $\omega = 2.364\times10^{14}$ rad·s, the xy-plane crosses the particle center; (c) same as (b) but for the xz-plane crossing the particle center.

average of the electric field at an arbitrary position $\mathbf{r}$ above the substrate, using the fluctuational electrodynamics, can be calculated by[24]

$$\langle|\mathbf{E}(\mathbf{r})|^2\rangle = \frac{4\pi k_0^4}{\varepsilon_0\omega}\Theta(\omega, T)\mathrm{Tr}\left[\hat{G}(\mathbf{r}, \mathbf{r}_0)\hat{\chi}\hat{G}(\mathbf{r}, \mathbf{r}_0)^\dagger\right], \quad (6)$$

where k_0 is the free-space wave number, ε_0 is the vacuum permittivity, $\mathbf{r}_0$ is the position of the particle, $\hat{\chi}$ is the related to the electric polarizability tensor by $\hat{\chi} = (\hat{\alpha} - \hat{\alpha}^\dagger)/2\mathrm{i}$, and $\hat{G}(\mathbf{r}, \mathbf{r}_0)$ is the total Green's tensor composed of the free space and the reflection parts (see the supplementary material for details), i.e.,

$$\hat{G}(\mathbf{r}, \mathbf{r}_0) = \hat{G}^0(\mathbf{r}, \mathbf{r}_0) + \hat{G}^R(\mathbf{r}, \mathbf{r}_0). \quad (7)$$

Note that Eq. (6) does not account for the multiple scattering between the nanoparticle and the substrate, which is negligibly small in this case. Figures 2(b) and 2(c) demonstrate the spatial distribution of the averaged emitting electric field $\langle|\mathbf{E}(\mathbf{r})|\rangle$ at the angular frequency $\omega = 2.364 \times 10^{14}$ rad·s in the xy- and xz-planes crossing the particle center. As shown, there is a region of strong electric fields near the particle and the substrate, but the distribution pattern is clearly asymmetric with respect to the plane of $x = 0$, i.e., the region of strong electric fields is larger in the $x > 0$ half space. This indicates that the emitted light of the WSM nanoparticle excites the surface modes of the c-BN substrate, which are unidirectional due to the spin-directional coupling between the localized circular mode of the nanoparticle and the propagating surface modes of the substrate.

Then we consider the impact of this spin-directional coupling on the far-field thermal emission and absorption of WSM nanoparticles. To evaluate the emission and absorption of WSM nanoparticles, we use the directional and spectral emission $Q_e(\omega, \hat{\mathbf{r}})$ and absorption $Q_a(\omega, \hat{\mathbf{r}})$ efficiencies. According to the derivations in the thermal discrete dipole approximation for MO particles,[24] the thermal emission of certain polarization by a collection of N electric dipoles in the presence of a substrate can be described by a cross section-like quantity that

$$C_{\mathrm{emi}}(\omega, \hat{\mathbf{r}}, \hat{\mathbf{e}}) = (4\pi r^2)k_0 Tr\left\{\mathbf{G}\bar{T}^{-1}\bar{\chi}\bar{T}^{-1\dagger}\mathbf{G}^\dagger\hat{\mathbf{e}}\hat{\mathbf{e}}_T\right\}, \quad (8)$$

where $\hat{\mathbf{e}}$ defines the polarization unit vector, r is a far-field distance, $\bar{\chi} = \mathrm{diag}(\hat{\chi}_1, \ldots, \hat{\chi}_N)$, $\mathbf{G} = [\hat{G}(\mathbf{r}, \mathbf{r}_1), \ldots, \hat{G}(\mathbf{r}, \mathbf{r}_N)]$, the matrix $\bar{T}$ is calculated by $\bar{T} = \bar{1} - k_0^2\bar{\alpha}\bar{G}$ with $\bar{\alpha} = \mathrm{diag}(\hat{\alpha}_1, \ldots, \hat{\alpha}_N)$, and the elements of $\bar{G}$ given by $\bar{G}_{ij} = [(1 - \delta_{ij})\hat{G}_0(\mathbf{r}_i, \mathbf{r}_j) + \hat{G}_R(\mathbf{r}_i, \mathbf{r}_j)]$. We emphasize that Eq. (8) considers the multiple scattering of the particles through direct and reflecting interactions. The directional spectral emission efficiency is thus defined as $Q_e = C_{\mathrm{emi}}/(N\pi R^2)$ The total absorption cross section C_{abs} of a set of dipoles is calculated by[25]

$$C_{\mathrm{abs}} = \frac{k_0}{\varepsilon_0^2|\mathbf{E}_0^2|}\sum_{i=1}^{N}\mathrm{Im}\left[\mathbf{p}_i \cdot \left(\hat{\alpha}_i^{-1}\mathbf{p}_i\right)^*\right], \quad (9)$$

where the induced dipole moments $\mathbf{p}_i$ of the nanoparticles are solved by the coupled dipole equation[25]

$$\mathbf{p}_i = \varepsilon_0\hat{\alpha}_i\mathbf{E}_{\mathrm{inc}}(\mathbf{r}_i) + k_0^2\hat{\alpha}_i\sum_j^N \bar{G}_{ij}\mathbf{p}_j, \quad (10)$$

in which the incident electric field $\mathbf{E}_{\mathrm{inc}}$ has to consider the reflection of the substrate (see the supplementary material). The absorption efficiency is defined as $Q_a = C_{\mathrm{abs}}/(N\pi R^2)$.

The spectral distribution of Q_e and Q_a at an emission angle of $\theta = 30°$ is depicted in Fig. 3, where the WSM nanoparticle is located $h = 100$ nm above the substrate with 2b along -y. In the vacuum case, the calculating results show that Q_e always equals to Q_a for both p- and s-polarizations. The differences between the efficiencies of the two polarizations are caused by the anisotropy of the WSM material.[22] In the presence of the c-BN substrate, the s-polarized $Q_{e,s}$ and $Q_{a,s}$ are substantially decreased but are still equal to each other; however, the p-polarized $Q_{e,p}$ and $Q_{a,p}$ are drastically different, $Q_{e,p}$ is greatly enhanced, and is much larger than $Q_{a,p}$, which is a sufficient evidence of the nonreciprocal emission and absorption of the WSM nanoparticle.

Figure 4(a) further demonstrates the directional and spectral region map of the averaged emission efficiencies (over p- and s-polarizations) of a WSM nanoparticle in the presence of the c-BN substrate. Large values of the emission efficiency are confined in a narrow spectral range, and their distribution is clearly asymmetric with respect to the angle $\theta = 0°$. Figure 4(b) depicts the hemispherical angular distribution of the emission efficiencies at $\omega = 2.29 \times 10^{14}$ rad·s, which clearly shows the angular asymmetry of the thermal emission. The spectral and angularly asymmetric distribution of the emission is not notably affected by near-field interactions of WSM nanoparticles, as indicated by similar region maps in Figs. 4(c) and 4(d) for a 5×5 lattice of WSM nanoparticles.

We note that Kirchhoff's law has been proved to be valid for isolated MO particles[26] or MO nanoparticle clusters,[22] in agreement with the vacuum cases in Fig. 3. However, the spin-directional coupling with reciprocal surface modes can break Kirchhoff's law[1] or the local form of Kirchhoff's law[27] of the WSM nanoparticles. This indicates that spin-directional coupling can be exploited to develop nonreciprocal thermal emitters. Despite the nonreciprocal emission and

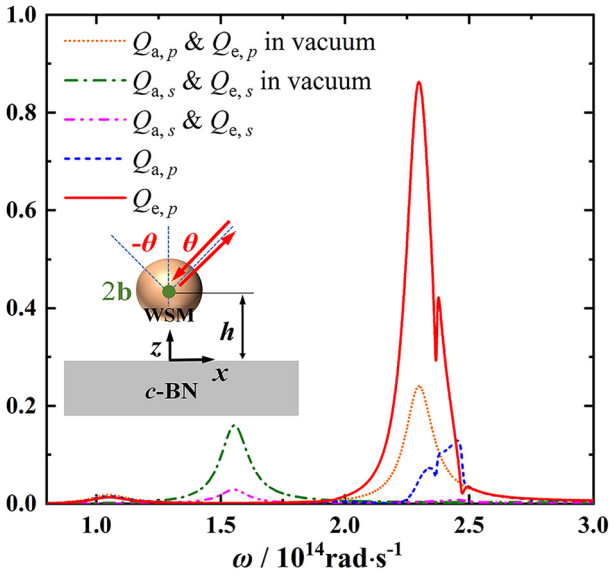

FIG. 3. The p- and s-polarized components of the emission efficiency $Q_e(\omega)$ and the absorption efficiency $Q_a(\omega)$ of a WSM nanoparticle ($R = 25$ nm) above the c-BN substrate by a distance $h = 100$ nm, the emission and incident angle is $\theta = 30°$; vacuum cases are added for comparison.

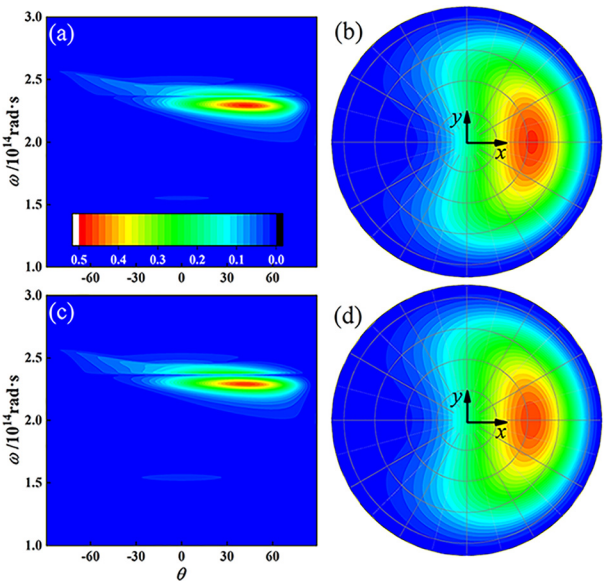

FIG. 4. (a) Directional and spectral region map of the averaged emission efficiency (over *p*- and *s*-polarizations) of a WSM nanoparticle; (b) hemispherical angular distribution of the averaged directional emission efficiency of a WSM nanoparticle at $\omega = 2.29 \times 10^{14}$ rad·s; (c) same as (a) but for a 5×5 WSM nanoparticle lattice (lattice length 100 nm) placed parallel to the *c*-BN substrate by $h = 100$ nm; (d) same as (b) but for the 5×5 WSM nanoparticle lattice.

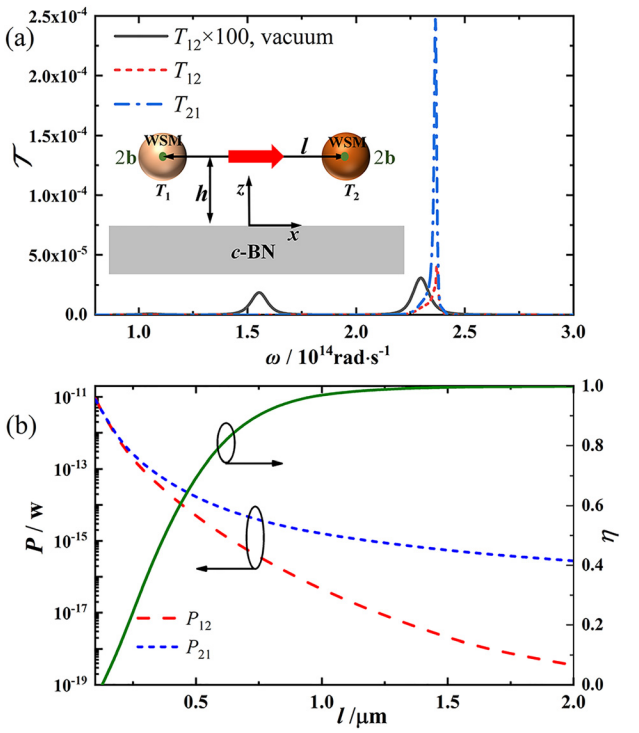

FIG. 5. RHT between two WSM nanoparticles (radius $R = 25$ nm, 2b along $-y$) located above a *c*-BN substrate by a distance $h = 100$ nm, (a) the spectral transfer coefficient $\mathcal{T}$, the distance between two particles is $l = 0.5$ μm; (b) total heat flux P as a function of l and the rectification ratio η.

absorption of the WSM nanoparticles, the thermodynamic equilibrium still holds since the large emission at $\theta > 0$ is balanced by the large absorption at $\theta < 0$. In fact, we found that the $Q_e(\omega, \theta)$ equals to $Q_a(\omega, -\theta)$ in all the cases considered (see the supplementary material).

We then advance to consider the near-field RHT between WSM nanoparticles in proximity to the *c*-BN substrate. The transmission coefficient between particles is calculated by[2,26]

$$\mathcal{T}_{ij} = \frac{4}{3} k_0^4 \mathrm{Tr}\left[\bar{\mathcal{G}}_{ij} \hat{\chi}_j \bar{\mathcal{G}}_{ij}^{\dagger} \hat{\chi}_i\right], \tag{11}$$

where the system Green's function $\bar{\mathcal{G}} = \bar{A}^{-1}\bar{G}$ with $\bar{A} = \bar{1} - k_0^2 \bar{G}\bar{\alpha}$. Equation (11) takes into account the multiple scattering of particles through direct and reflecting interactions.

Figure 5(a) shows the spectral transmission coefficients between two WSM nanoparticles (numbered as 1 and 2) separated by a distance $l = 500$ nm and located above the *c*-BN substrate by $h = 100$ nm. For the vacuum case, the transmission coefficients $\mathcal{T}_{12}(\omega)$ and $\mathcal{T}_{21}(\omega)$ always equal to each other. In the presence of the *c*-BN substrate, however, the transmission coefficients are orders of magnitude larger than those in vacuum (note the vacuum case is multiplied by 100 in Fig. 5), which is due to the near-field energy transport by the propagating surface modes.[28,29] Moreover, nonreciprocal RHT occurs since the transmission coefficients $\mathcal{T}_{12}(\omega)$ and $\mathcal{T}_{21}(\omega)$ are now drastically different, which is most remarkable in the Reststrahlen band of *c*-BN. The total radiative heat flux as a function of separation distance between the two particles is shown in Fig. 5(b). As shown, the radiative heat flux P_{21} is growingly larger than the reverse direction P_{12} with increasing l. For relatively larger separation distances (e.g., $l > 600$ nm), P_{21} is orders of magnitude larger than P_{12}. As a result, the rectification ratio η defined as $\eta = (P_{21} - P_{12})/P_{21}$ quickly approaches unity with increasing l. A radiative thermal dipole is thus established, and the difference to those in recent works[17,18] is that the surface modes are now reciprocal but unidirectionally excited. For detailed analysis of the RHT of the whole system (i.e., considering the background and the substrate), similar calculations can be conducted as those of Ott and Biehs,[19] where the spin-spin interactions with nonreciprocal surface waves are analyzed.

In conclusion, we have demonstrated the nonreciprocal far-field thermal emission and nonreciprocal near-field RHT of WSM nanoparticles due to the spin-directional coupling with reciprocal surface modes. We emphasize that the optical properties of WSMs can be tuned and the choice of the substrate material supporting surface modes is quite general; the circular thermal emission can also be realized by a topological insulator,[30] chiral nanostructures,[31] or nonequilibrium coupled antennas.[32] Thus, our work broadens the scope of exploring nonreciprocal thermal radiation, which is applicable to the design of nonreciprocal thermal emitters and to the nanoscale routing of the radiative heat flux. In addition, more possibilities in the thermal emission routing are expected if we replace the isotropic substrate by metasurfaces[33] that can be engineered with anisotropy, chirality, gyroptropy, and nonlocality.

See the supplementary material for Green's tensor, theoretical derivation, and the issues on thermodynamic equilibrium.

The support from the National Natural Science Foundation of China (Nos. 51906128 and 52076123) is acknowledged. J. Dong also acknowledges the support from the National Science Foundation of Shandong Province (No. ZR2019BEE011) and the China Postdoctoral Science Foundation.

DATA AVAILABILITY

The data that support the findings of this study are available within the article.

REFERENCES

[1]G. Kirchhoff, Ann. Phys. **185**, 275 (1860).
[2]P. Ben-Abdallah, S.-A. Biehs, and K. Joulain, Phys. Rev. Lett. **107**(11), 114301 (2011).
[3]S. Fan, Joule **1**(2), 264 (2017).
[4]L. Zhu and S. Fan, Phys. Rev. B **90**(22), 220301 (2014).
[5]B. Zhao, Y. Shi, J. Wang, Z. Zhao, N. Zhao, and S. Fan, Opt. Lett. **44**(17), 4203 (2019).
[6]X. Wu, ES Energy Environ. **12**, 46 (2021).
[7]B. Zhao, C. Guo, C. A. C. Garcia, P. Narang, and S. Fan, Nano Lett. **20**(3), 1923 (2020).
[8]Y. Tsurimaki, X. Qian, S. Pajovic, F. Han, M. Li, and G. Chen, Phys. Rev. B **101**(16), 165426 (2020).
[9]S. Pajovic, Y. Tsurimaki, X. Qian, and G. Chen, Phys. Rev. B **102**(16), 165417 (2020).
[10]O. V. Kotov and Y. E. Lozovik, Phys. Rev. B **93**(23), 235417 (2016).
[11]O. V. Kotov and Y. E. Lozovik, Phys. Rev. B **98**(19), 195446 (2018).
[12]P. Ben-Abdallah, Phys. Rev. Lett. **116**(8), 084301 (2016).
[13]L. Zhu and S. Fan, Phys. Rev. Lett. **117**(13), 134303 (2016).
[14]L. Zhu, Y. Guo, and S. Fan, Phys. Rev. B **97**(9), 094302 (2018).
[15]C. Guo, Y. Guo, and S. Fan, Phys. Rev. B **100**(20), 205416 (2019).
[16]A. Ott, S.-A. Biehs, and P. Ben-Abdallah, Phys. Rev. B **101**(24), 241411 (2020).
[17]A. Ott, R. Messina, P. Ben-Abdallah, and S.-A. Biehs, Appl. Phys. Lett. **114**(16), 163105 (2019).
[18]Y. Zhang, C.-L. Zhou, H.-L. Yi, and H.-P. Tan, Phys. Rev. Appl. **13**(3), 034021 (2020).
[19]A. Ott and S.-A. Biehs, Phys. Rev. B **101**(15), 155428 (2020).
[20]K. Y. Bliokh, F. J. Rodríguez-Fortuño, F. Nori, and A. V. Zayats, Nat. Photonics **9**(12), 796 (2015).
[21]A. Ott, P. Ben-Abdallah, and S.-A. Biehs, Phys. Rev. B **97**(20), 205414 (2018).
[22]J. Dong, W. Zhang, and L. Liu, J. Quant. Spectrosc. Radiat. Transfer **255**, 107279 (2020).
[23]E. D. Palik, *Handbook of Optical Constants of Solids* (Academic Press, New York, 1998).
[24]R. M. A. Ekeroth, P. Ben-Abdallah, J. C. Cuevas, and A. García-Martín, ACS Photonics **5**(3), 705 (2018).
[25]B. T. Draine, Astrophys. J. **333**(2), 848 (1988).
[26]R. M. A. Ekeroth, A. García-Martín, and J. C. Cuevas, Phys. Rev. B **95**(23), 235428 (2017).
[27]J.-J. Greffet, P. Bouchon, G. Brucoli, and F. Marquier, Phys. Rev. X **8**(2), 021008 (2018).
[28]J. Dong, J. Zhao, and L. Liu, Phys. Rev. B **97**(7), 075422 (2018).
[29]R. Messina, S.-A. Biehs, and P. Ben-Abdallah, Phys. Rev. B **97**(16), 165437 (2018).
[30]E. Khan and E. E. Narimanov, Phys. Rev. B **100**(8), 081408 (2019).
[31]S. A. Dyakov, V. A. Semenenko, N. A. Gippius, and S. G. Tikhodeev, Phys. Rev. B **98**(23), 235416 (2018).
[32]C. Khandekar and Z. Jacob, Phys. Rev. Appl. **12**(1), 014053 (2019).
[33]Y. Mazor and A. Alù, Phys. Rev. Appl. **14**(1), 014029 (2020).